Journal of Applied Polymer Science

WILEY

Applied Polymer SCIENCE

RESEARCH ARTICLE OPEN ACCESS

Hybrid Flexible Dry Electrodes for Electroencephalography: Electrical and Thermo-Mechanical Properties

George Gnonhoue | Éric David | Jérémie Voix | Ilyass Tabiai

Université du Québec, École de Technologie Supérieure, Montreal, Quebec, Canada

Correspondence: George Gnonhoue (olatoundji-george.gnonhoue.1@ens.etsmtl.ca) | Ilyass Tabiai (ilyass.tabiai@etsmtl.ca)

Received: 15 August 2025 | **Revised:** 12 November 2025 | **Accepted:** 18 November 2025

Keywords: applications | dielectric properties | mechanical properties | sensors and actuators | thermogravimetric analysis (TGA)

ABSTRACT

This study evaluates styrene–ethylene–butylene–styrene (SEBS) composites modified with carbon nanotubes (CNTs) and carbon black (CB) for flexible electroencephalography (EEG) electrodes. Maleic anhydride-grafted SEBS (SEBS-MA) with 8 wt% CNTs and 2 wt% CB provides an optimal balance of conductivity and flexibility, a storage modulus comparable to SEBS, and yields a highly flexible conductive material. SEBS and SEBS-MA composites with 8 wt% CNT/2 wt% CB produced stable, low-noise signals, suggesting responsiveness to brain activity. The contact impedance of the elastomeric thermoplastic polymer (SEBS)/8 wt% CNT/2 wt% CB electrode is 4.25 ± 0.5 kΩ, and 4.5 ± 0.6 kΩ for SEBS-MA/8 wt% CNT/2 wt% CB, comparable to a commercial electrode (4.75 ± 1.5 kΩ). SEBS/8 wt% CNT/2 wt% CB and SEBS-MA/8 wt% CNT/2 wt% CB produced stable, low-noise EEG signals. In vivo EEG recordings demonstrated that SEBS-MA with 8 wt% CNT/2 wt% CB effectively captured transitions between the eyes-open and eyes-closed states, yielding clear and stable signals. These findings suggest that SEBS-MA/8 wt% CNT/2 wt% CB is a promising material for flexible, high-performance EEG electrodes due to its balance of electrical conductivity, mechanical stability, and signal clarity.

1 | Introduction

Electroencephalography (EEG) is a noninvasive technique that records brain electrical activity through electrodes placed on the scalp [1–4]. Conventional EEG systems rely on wet electrodes, which use a conductive gel to reduce electrode–skin impedance to values typically in the range of 5–10 kΩ [5, 6]. This ensures high-quality signal acquisition; however, gel electrodes present significant drawbacks. The gel dries out over time, causing impedance to rise and signal degradation, and their application and removal are inconvenient and uncomfortable for the user [7]. These limitations restrict their suitability for long-term and portable EEG applications.

To overcome these challenges, research has focused on the development of dry electrodes, which operate without the need for gel [8]. Three main categories exist: microneedle electrodes, which penetrate the stratum corneum and can achieve impedances as low as 10–50 kΩ [1, 9], but may cause discomfort and biocompatibility concerns; capacitive electrodes, which record signals through an insulating layer and allow noncontact acquisition, but often suffer from impedances above 200 kΩ and are highly sensitive to motion artifacts [10–14]; and surface electrodes, which contact the skin directly and offer a more user-friendly solution with relatively simple fabrication steps, though they typically present impedances above the 20 kΩ range [15, 16].

Most modern surface dry electrodes depend on thin conductive coatings applied to a polymer substrate. These coatings can deteriorate or peel off after repeated use, reducing performance [17–23]. To address this limitation, bulk conductive composites have been developed, in which electrical conductivity is embedded throughout the electrode rather than only at the surface [24]. Conductivity is generally achieved by incorporating

carbon-based fillers such as carbon black (CB) or carbon nanotubes (CNTs) [25]. CB and CNTs each present distinct advantages and limitations when used individually as conductive fillers. CB is low-cost and widely available, but requires high loadings to reach percolation [26], which increases stiffness. CNTs enable high conductivity at lower loadings and can reduce contact impedance below, but their addition tends to stiffen the polymer matrix and reduce flexibility [27].

To overcome these trade-offs, several studies have proposed the development of hybrid electrodes, in which two or more fillers are incorporated into the same polymer matrix. The rationale is that the complementary properties of different fillers can be exploited. This synergistic effect has been shown to lower the overall percolation threshold, improve electrical stability, and reduce the need for excessively high filler loadings [28–33]. Nevertheless, the primary challenge remains optimizing the fabrication process. Achieving the right balance between filler fraction, dispersion quality, and electrical performance is critical to ensuring that electrodes are both conductive and mechanically compliant. Excessive filler loading leads to stiffness and discomfort, while insufficient loading compromises conductivity and increases impedance.

The choice of polymer matrix also plays a central role. Blends of polydimethylsiloxane (PDMS) and thermoplastic polymer (TPU), reinforced with materials such as CNT and CB, graphene, and silver nanowires, are commonly used to fabricate hybrid composites for flexible sensors that detect human movements [23, 30, 31, 34–41]. PDMS offers softness and biocompatibility; however, its excessive flexibility leads to unstable electrode–skin contact, resulting in impedance fluctuations [42, 43]. TPU, on the other hand, offers mechanical robustness but can sometimes be too rigid for comfortable long-term wear [18, 44, 45]. Consequently, alternative matrices such as styrene–ethylene–butylene–styrene (SEBS) have attracted attention. SEBS is a thermoplastic elastomer that combines soft and hard phases: the soft phase provides skin conformity and comfort, while the complex domains stabilize contact under mechanical pressure at the surface of the electrodes [28, 33, 46–48]. Furthermore, maleic anhydride-grafted SEBS (SEBS-MA) enhances filler dispersion and interfacial adhesion, potentially reducing the high stiffness of composites [49, 50].

To develop flexible, comfortable EEG electrodes with stable, low impedance, we explore SEBS/CNT/CB and SEBS-MA/CNT/CB hybrid nanocomposites, designed to leverage the complementary properties of CNT and CB while avoiding the high filler loadings and mechanical stiffness typically associated with single-filler systems. In this study, we investigate these hybrid nanocomposites as bulk conductive materials for dry surface EEG electrodes. Previous research on SEBS/CB and SEBS/CNT composites has shown low contact impedance at high filler loadings—specifically 20 wt% CB (despite a percolation threshold above ~12 wt%) and 16 wt% CNT (despite a percolation threshold near ~3 wt%). However, such high filler levels can reduce flexibility and comfort. By combining CNT and CB, synergistic conductive networks can form, allowing for reduced filler content while maintaining conductivity and lowering electrode–skin impedance below clinically relevant levels ($< 5\,k\Omega$). The addition of SEBS-MA enhances filler dispersion and polymer–nanoparticle interactions, potentially alleviating stiffness. These hybrid nanocomposites were prepared through solvent dissolution and systematically evaluated for morphology, dispersion, electrical conductivity, and EEG performance, to create durable, flexible, low-impedance electrodes that address the limitations of traditional wet and coated dry electrodes.

2 | Materials and Methods

2.1 | Materials

The materials used in this study were chosen for their suitability in flexible EEG electrode applications. SEBS, an elastomeric thermoplastic polymer with a number-average molecular weight of 54,000 g/mol and a polystyrene (PS) content of 30 wt%, was supplied by Kraton (Paulínia, SP, Brazil). Maleic anhydride-grafted SEBS (SEBS-MA), also obtained from Kraton, was used to improve the interaction between the polymer matrix and conductive fillers.

Multiwalled carbon nanotubes (MWCNTs), NC 7000 grade, were obtained from Nanocyl S.A. (Sambreville, Belgium). These nanotubes have an average diameter of 9.5 nm, an average length of 1.5 μm, a surface area ranging from 250 to 300 m^2/g, a nominal electrical conductivity of 100 S/m, a density between 1.30 and 2.00 g/cm^3, and a carbon purity of at least 90%.

CB, Lampblack type C198-500 (Lot 145509), was obtained from Fisher Chemical (Fisher Scientific, Ottawa, ON, Canada). It consists of nanoparticles approximately 50 nm in size, with a nominal electrical conductivity of 400 S/m and a density of 1.8 g/cm^3.

For solution processing, toluene (UN1294, Optima, T291-4, Lot 234238) was purchased from Fisher Chemical (Fisher Scientific Company, Ottawa, ON, Canada).

2.2 | Composite Preparation

Electrode composites were created using a solution-casting and compression-molding process (see schematic in Figure 1).

Polymer Dissolution: SEBS or SEBS-MA pellets were dissolved in toluene at 100°C with magnetic stirring at 600 rpm until a clear, homogeneous solution formed.

Filler Incorporation: CNT and CB were added to the polymer solution at specified weight fractions (Tables 1 and 2). Dispersion was maintained through continuous stirring at 100°C for 30 min to ensure uniform distribution of the filler.

Solvent Evaporation: The suspension was cast and left to dry under a fume hood at room temperature until all solvent evaporated, resulting in nanocomposite films.

Electrode Molding: The dried films were compression molded into multipin electrode geometries using a heated press at 215°C.

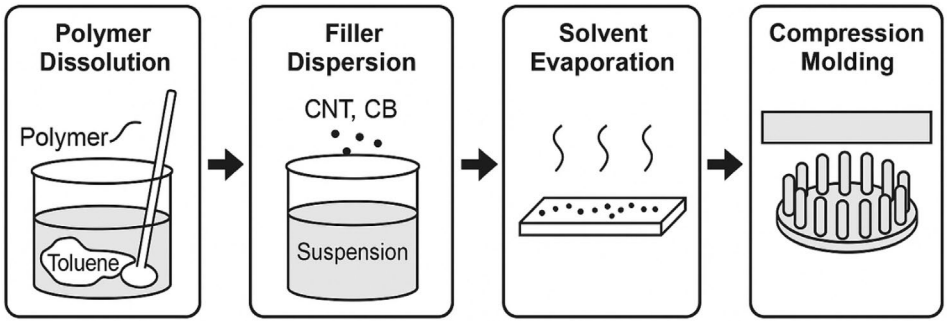

FIGURE 1 | Schematic overview of the fabrication process for flexible multipin dry electrodes. The method includes (i) dissolving the SEBS or SEBS-MA polymer in toluene, (ii) dispersing conductive fillers (CNT and CB) to create a uniform suspension, (iii) evaporating the solvent to form composite films, and (iv) using compression molding to shape the films into multipin electrode structures.

TABLE 1 | Composition of styrene–ethylene–butylene–styrene (SEBS) nanocomposites with different weight fractions (wt%) of carbon nanotubes (CNTs) and carbon black (CB).

Reinforcements		
CNT	**CB**	**Matrix**
—	—	100
3	2	95
8	2	90
10	—	90
—	10	90
10	5	85
16	—	84
15	5	80
—	20	80

TABLE 2 | Composition of maleic anhydride-grafted styrene–ethylene–butylene–styrene (SEBS-MA) nanocomposites with different weight fractions of carbon nanotubes (CNTs) and carbon black (CB).

Reinforcements		
CNT	**CB**	**Matrix**
—	—	100
3	2	95
8	2	90
10	—	90
—	10	90
10	5	85
16	—	84
15	5	80
—	20	80

The process involved an initial pressure of 0.8 MPa for 5 min, followed by a pressure of 5 MPa for 15 min.

2.3 | Electrode Geometry

Each electrode consisted of 19 cylindrical pins arranged in a circular pattern. The pins had an average height of 4.9 ± 0.09 mm and a diameter of 1.41 ± 0.01 mm. The center-to-center distance between neighboring pins was about 2.5 mm, which corresponds to an edge-to-edge spacing of approximately 1.1 mm at the electrode–skin interface.

2.4 | Composite Formulations

The compositions of the prepared composites are summarized in Tables 1 and 2. For each formulation, three independent samples were fabricated and characterized to ensure reproducibility. Comparative analyses were conducted between SEBS/CNT/CB and SEBS-MA/CNT/CB composites at equivalent filler loadings to determine the most suitable material for EEG applications.

3 | Characterization

3.1 | Electrical Characterization

Electrical conductivities of the composites were measured using a frequency-domain broadband dielectric spectrometer (Alpha-A Dielectric Analyzer, Novocontrol, Montabaur, Germany). Disks with a 20 mm diameter and a thickness of 1.2 mm were placed between two solid brass electrodes, creating a plane-plane electrode/composite material/electrode sandwich. The measurements were performed over a frequency range from 10^2 Hz to 10^5 Hz at 30°C.

3.2 | Structural Characterization

The composite morphology was examined with a high-resolution scanning electron microscope (SEM, Hitachi SU-8230 field-emission SEM) operated at 5 kV to evaluate the dispersion of

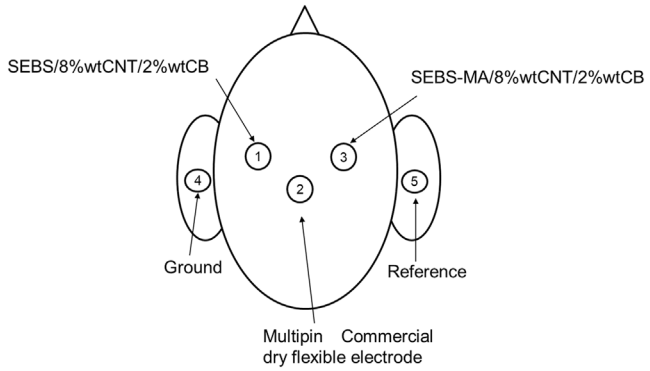

FIGURE 2 | Schematic of electrode placement on the scalp using the Ultracortex "Mark IV" EEG headset. Multipin flexible electrodes developed in this work were positioned at sites 1 (left) and 3 (right), while a commercial dry flexible electrode (OpenBCI, USA) was placed at site 2 for comparison. Electrodes 4 and 5, located near the ears, served as ground and reference.

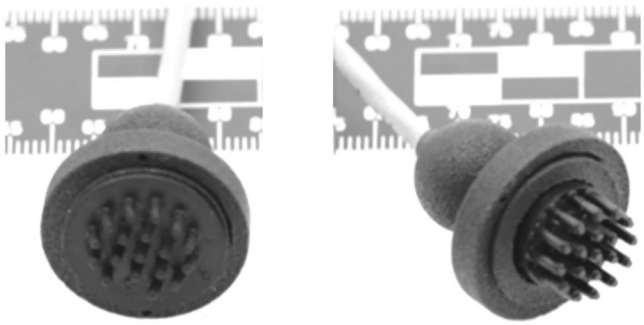

FIGURE 3 | Photos of the electrodes used in this study. (Left) Commercial dry flexible electrode from OpenBCI (New York, NY, USA), used as a reference. (Right) Multipin flexible electrode developed in this work, side view. The built-in ruler shows the scale for electrode sizes.

conductive fillers within the matrix. Cross-sections were prepared using a microtome and sputter-coated with approximately 2 nm of platinum using a turbo-pumped sputter/carbon coater (Quorum Technologies Q150T).

3.3 | Thermo-Mechanical Characterization

Thermogravimetric analysis (TGA) was performed using a Diamond TG/differential thermal analysis (DTA) system (PerkinElmer) to determine the filler weight fractions and decomposition temperatures of the composites. Approximately 10–13 mg of material was heated from 20°C to 500°C at a rate of 3°C/min under a nitrogen flow of 100 mL/min, followed by a 2-min isothermal hold at 500°C.

Differential scanning calorimetry (DSC) was used to examine the thermal properties of the pure polymer matrices (SEBS and SEBS-MA). Tests were carried out in a nitrogen atmosphere to prevent oxidation. Approximately 10 mg samples were sealed in aluminum pans and heated at a rate of 10°C/min. To prevent thermal degradation, the measurement ranges were adjusted based on the thermal stability of each material: −100°C to 220°C for SEBS and −100°C to 320°C for SEBS-MA. These conditions allowed for the detection of key transitions, including the glass transitions of both the soft and hard phases, without interference from decomposition.

Dynamic mechanical thermal analysis (DMTA) of SEBS-MA/CNT/CB and SEBS/CNT/CB composites was performed using a Q800 instrument (TA Instruments Inc.) with a double cantilever clamp (22 mm frame, 2 mm center clamp). Rectangular specimens (8 mm wide, 2 mm thick) were tested at a strain of 0.4%, a frequency of 1 Hz, and a heating rate of 2°C/min across 25°C–35°C. Measurements were conducted under laboratory conditions (~23°C, 45%–55% relative humidity). The storage modulus was solely evaluated to assess stiffness and elastic behavior within this temperature range.

3.4 | Preliminary In Vivo Validation

Multipin flexible EEG electrodes were tested for contact impedance and EEG recording on hairy scalp areas to mimic real-world application conditions. This method was selected to evaluate both the electrode's performance and that of commercial alternatives.

Recordings were wirelessly collected using an OpenBCI 16-channel Cyton Biosensing Board embedded in the Ultracortex "Mark IV" EEG headset (OpenBCI, New York, NY, USA). This headset allows for comfortable electrode placement with minimal pressure, ensuring consistent positioning according to the international 10-20 system.

Contact impedance and EEG signal amplitude from the newly developed multipin electrodes at positions 1 and 3 (Figure 2) were compared to those from a commercial dry flexible electrode (OpenBCI, New York, NY, USA) placed at site 2. Measurements were taken on a healthy volunteer using a setup that included the developed electrode, a reference, and a ground, with impedance recorded between the test and reference electrodes.

To evaluate EEG signal quality, participants sat in a quiet room while recordings were taken for 10 s. Following standard protocols and the recommendations of the American Clinical Neurophysiology Society [51], participants were instructed to minimize head and facial muscle activity and remain still to reduce movement artifacts. This method enabled reliable detection of eye-blink reflex artifacts and neural oscillations.

The Ultracortex "Mark IV" headset is designed to ensure consistent and precise electrode placement on the scalp, thereby improving the reliability of EEG measurements and reducing variability in data collection. The headset features adjustable arms and labeled slots that align electrodes according to the international 10-20 system. Figure 3 shows the electrodes developed in this work alongside the commercial flexible electrode from OpenBCI, which was used as a performance benchmark.

3.4.1 | Participants

Participant testing was conducted to evaluate the performance of the developed EEG electrodes under physiological conditions,

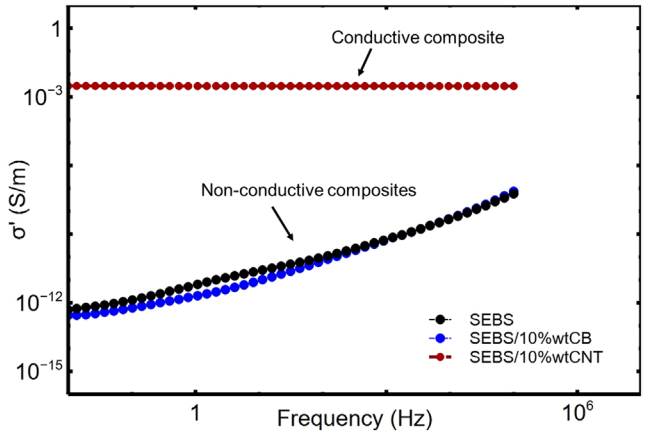

FIGURE 4 | Electrical conductivities of SEBS/10 wt% CNT versus SEBS/10 wt% CB (σ' vs. frequency). [Color figure can be viewed at wileyonlinelibrary.com]

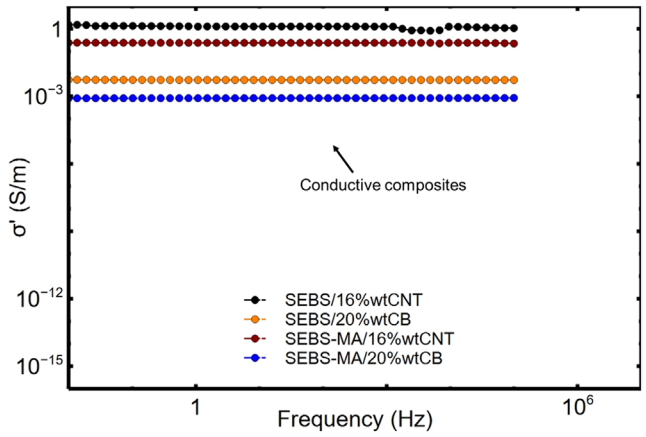

FIGURE 5 | Electrical conductivity of SEBS/16 wt% CNT, SEBS/20 wt% CB, SEBS-MA/16 wt% CNT, and SEBS-MA/20 wt% CB (σ' vs. frequency). [Color figure can be viewed at wileyonlinelibrary.com]

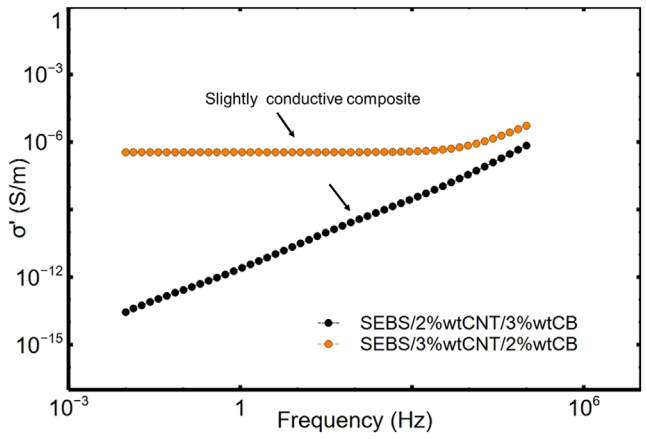

FIGURE 6 | Hybrid SEBS composites with 5 wt% total reinforcement (σ' vs. frequency). [Color figure can be viewed at wileyonlinelibrary.com]

with a focus on signal quality and motion artifacts. Healthy adult volunteers ($n = 4$; 1 male, 3 females; age range 21–35 years) participated in EEG measurements.

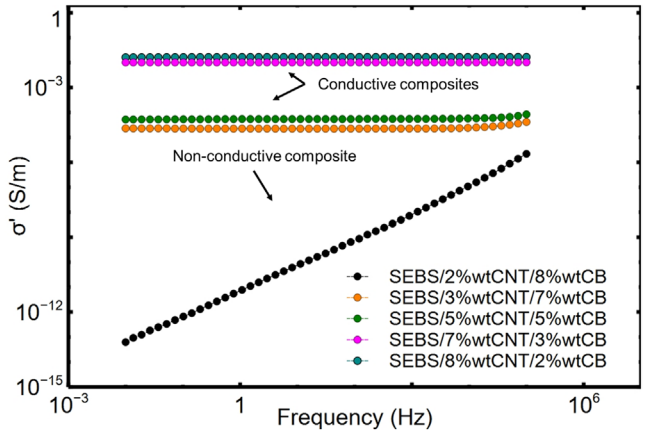

FIGURE 7 | Hybrid SEBS composites with 10 wt% total reinforcement showing CNT content-controlled transition to frequency-independent behavior (σ' vs. frequency). [Color figure can be viewed at wileyonlinelibrary.com]

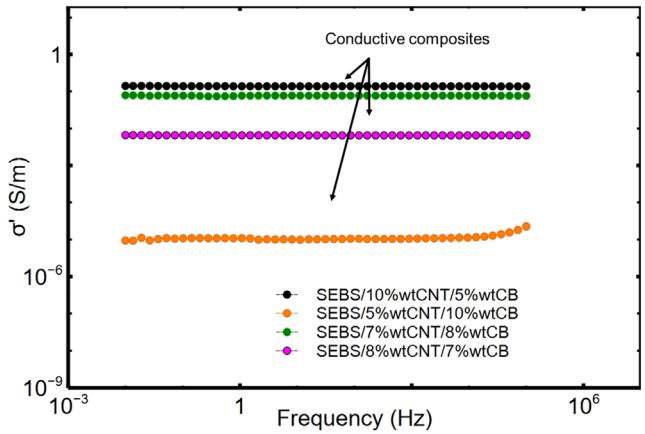

FIGURE 8 | Hybrid SEBS composites with 15 wt% total reinforcement (σ' vs. frequency). [Color figure can be viewed at wileyonlinelibrary.com]

All procedures were approved by the ÉTS Internal Review Board (Comité d'éthique de la recherche, Approval No. H20230504) and conducted in accordance with the principles outlined in the Declaration of Helsinki. Written informed consent was obtained from all participants before the experiments.

4 | Results

4.1 | Electrical Properties

Figures 4–10 summarize the real part of the complex conductivity, $\sigma'(f)$, for SEBS and SEBS-MA composites filled with CNT, CB, and CNT/CB hybrids.

4.1.1 | Frequency Response and Filler-Morphology Effects

Figure 4 shows that SEBS/10 wt% CNT is already a conductive composite ($\sigma' \approx 10^{-2}$–10^{-3} S·m^{-1}, with a frequency-independent plateau), whereas SEBS/10 wt% CB remains insulating

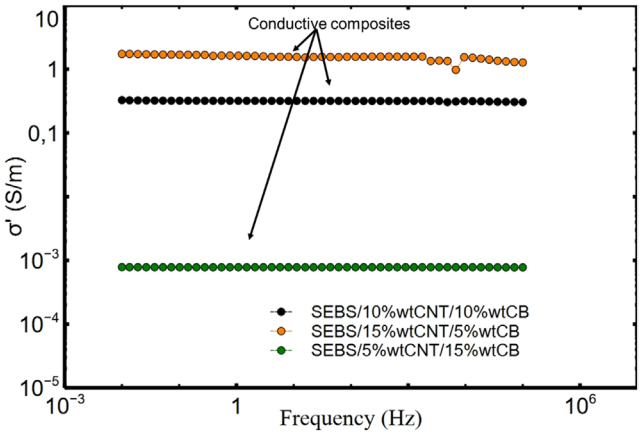

FIGURE 9 | Hybrid SEBS composites at 20 wt% total reinforcement (σ′ vs. frequency). [Color figure can be viewed at wileyonlinelibrary.com]

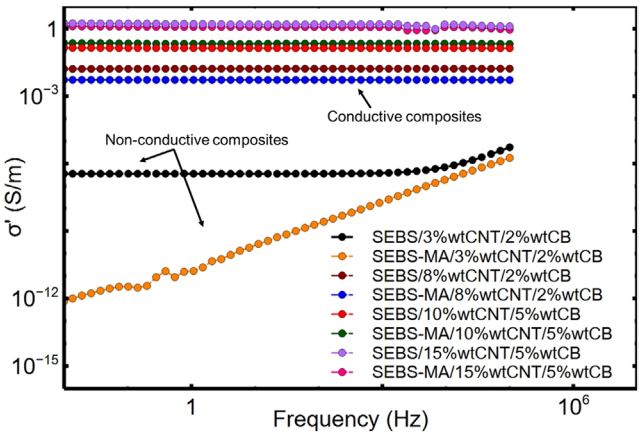

FIGURE 10 | Modifying with maleic anhydride reduces conductivity compared to SEBS at the same CNT/CB loadings (σ′ vs. frequency), with no advantageous shift in percolation for these systems. [Color figure can be viewed at wileyonlinelibrary.com]

($\sigma' \approx 10^{-12}$ S·m^{-1} at 1 Hz with strong dispersion). The higher aspect ratio of CNT encourages the formation of a connected network at much lower loadings than quasi-spherical CB. The differences highlight how filler shape influences charge transport pathways. CNTs, due to their high aspect ratio and intrinsic conductivity, tend to form more efficient percolation networks at lower loadings compared to CB, which comprises nearly spherical particles with a lower surface area-to-volume ratio. In this context, σ' refers to the real part of the complex electrical conductivity (σ), which measures the material's ability to conduct electricity through ion movement. It excludes the imaginary part (σ''), which accounts for capacitive or inductive responses related to energy storage. Therefore, σ' provides a direct measure of the composite's effective electrical performance, which is crucial for applications like dry EEG electrodes, where both high conductivity and long-term stability are essential.

Figure 5 compares high-loading systems: SEBS/16 wt% CNT reaches about 1 S·m^{-1} with a flat plateau, SEBS/20 wt% CB reaches roughly 10^{-2} S·m^{-1}, and the SEBS-MA counterparts are consistently lower at the same filler levels (see below). The electrical conductivity data in Figure 5 demonstrate how reinforcement loading affects the conductivity of both SEBS and SEBS-MA matrices, offering insights into the percolation threshold and electron transport mechanisms within the composites. The electrical conductivity of SEBS and SEBS-MA composites with reinforcement weight fractions of 10%, 16%, and 20% is shown in Figures 4 and 5, illustrating distinct conductivity behaviors based on filler type and concentration.

Table 3 summarizes the electrical conductivity of SEBS and SEBS-MA composites at different reinforcement loadings, complementing Figures 4 and 5 by highlighting the role of CNT and CB in determining conductive network formation.

Hybrid series (Figures 6–9) confirm that CNT-rich blends control network formation and flatten the frequency response; in

TABLE 3 | Electrical conductivity of SEBS and SEBS-MA composites with different CNT and CB loadings (see Figures 4 and 5).

Composite formulation	Conductivity at 1 Hz (S/m)	Frequency dependence	Interpretation
Neat SEBS (unfilled)	~10^{-12}	Strong increase with frequency	Typical insulating behavior
SEBS/10 wt% CB	~10^{-12}	Increases significantly with frequency	CB is insufficient to form a conductive network at 10 wt%
SEBS/10 wt% CNT	10^{-3}–10^{-2}	Frequency-independent	Stable conductive network from CNTs
SEBS/16 wt% CNT	~1	Frequency-independent	A strong CNT network guarantees reliable conduction
SEBS/20 wt% CB	~10^{-2}	Frequency-independent	Continuous CB network established at 20 wt%
SEBS-MA/16 wt% CNT	10^{-1}–~1	Frequency-independent	Slightly lower conductivity than SEBS/16% CNT; CNT network is somewhat less efficient
SEBS-MA/20 wt% CB	~10^{-3}	Frequency-independent	Lower than SEBS/20% CB; MA modification does not improve conduction

TABLE 4 | Electrical conductivity of SEBS composites (10 wt% reinforcement) with different CNT/CB ratios.

Composite formulation	Conductivity at 1 Hz (S/m)	Frequency dependence	Interpretation
2% CNT/3% CB	~10^{-12}	Strong increase with frequency	Weak network, CB-dominated; poor continuous paths
3% CNT/2% CB	~10^{-6}	Slight increase after 10^3 Hz	CNT-dominated robust network; significantly higher conductivity than 2% CNT/3% CB
3% CNT/7% CB	~10^{-5}	Slight increase	Moderate network, improved vs. 2% CNT/3% CB
5% CNT/5% CB	~10^{-4}	Slight increase	Higher conductivity than 3% CNT/7% CB
7% CNT/3% CB	~10^{-2}	Stable (frequency-independent)	Strong CNT-dominated network; robust conduction
8% CNT/2% CB	> 10^{-2}	Stable (frequency-independent)	Highly efficient CNT network; minimal CB contribution

contrast, CB alone or CB-rich blends require significantly higher total loadings and still exhibit lower plateaus. For dry electrodes, $\sigma' \geq 10^{-2}$ S·m^{-1} with minimal frequency dependence around 31 Hz is desirable. CNT-rich SEBS (≥ 7–8 wt% CNT with a small CB fraction) meets this target, while CB-rich systems do not. Figure 6 compares the conductivity of SEBS composites with reinforcement weight fractions of 5%. It illustrates the conductivity of SEBS composites with 5% reinforcement weight fractions as a function of frequency.

The data show the baseline conductivity achieved at this low reinforcement loading, serving as a reference to compare with higher reinforcement concentrations. Figure 7 compares the conductivity of SEBS composites with 10% reinforcement weight fractions. It presents the conductivity of SEBS composites with 10% reinforcement as a function of frequency.

Figure 7 shows the electrical conductivity of SEBS composites containing 10% by weight of reinforcement. This concentration shows a significant increase in conductivity compared to lower concentrations, indicating the formation of conductive pathways within the composite material.

Table 4 summarizes the electrical conductivity values and frequency-dependent behavior of SEBS composites containing a total of 10 wt% reinforcement with different CNT/CB ratios, complementing the results shown in Figure 7.

Figure 8 displays SEBS composites with a 15% weight fraction, comparing their conductivity as a function of frequency across different amounts of carbon nanotubes (CNTs) and carbon black (CB).

The electrical conductivity of SEBS composites with a 15% weight fraction of reinforcement at this level indicates a well-connected conductive network within the SEBS matrix. Figure 9 shows SEBS composites with 20% weight reinforcement, comparing the conductivity of SEBS composites with different amounts of carbon nanotubes (CNTs) and CB as a function of frequency.

The electrical conductivity of SEBS composites with 20% weight of reinforcement exhibits a high level of conductivity, confirming the formation of a continuous and effective conductive network throughout the material. Table 5 summarizes the electrical conductivity and frequency-dependent behavior of SEBS composites with 20 wt% total reinforcement, highlighting the influence of CNT/CB ratios as shown in Figure 9.

The greater effectiveness of CNT in forming a conductive network, compared to CB, results in higher conductivity and less frequency dependence. Combining CNT and CB can be fine-tuned to achieve specific electrical properties. A higher CB content, without sufficient CNTs to form synergistic networks, results in lower overall conductivity in SEBS composites. This maintains consistent conductivity across frequencies, highlighting the efficiency of CNTs in creating a conductive network compared to CB. Although CB contributes to conductivity, its effect is less significant than that of CNTs, especially at higher concentrations. Excess CB without sufficient CNT can cause lower overall conductivity. The conductivity of SEBS composites is heavily influenced by the ratio of CNTs to CB; CNTs are crucial for establishing effective conductive networks, while CB plays a secondary role. Figure 10 compares the electrical conductivities (in S/m) of SEBS-MA composites with those of highly conductive SEBS composites across different frequencies. The data highlight the impact of varying CNT and CB concentrations in SEBS and SEBS-MA composites. Each line in the graph represents a specific combination of SEBS/SEBS-MA, CNT concentration, and CB concentration.

The electrical conductivity data in Figure 10 illustrates how both matrix type and reinforcement loading influence overall conductivity, providing insights for designing composites with better electrical properties. Table 6 compares the electrical conductivity of SEBS and SEBS-MA composites, showing that maleic anhydride modification generally reduces conductivity across various CNT/CB loadings, as demonstrated in Figure 10.

TABLE 5 | Electrical conductivity and frequency-dependent behavior of SEBS composites with 20 wt% CNT/CB reinforcement (see Figure 9).

Composite formulation	Conductivity at 1 Hz (S/m)	Frequency dependence	Interpretation
10% CNT/5% CB	$>10^{-1}$	Stable (frequency-independent)	High CNT forms a robust network; CB adds extra contribution
5% CNT/10% CB	~10^{-5}	Slight increase at high frequencies	Less efficient network due to lower CNT content
7% CNT/8% CB	~10^{-1}	Stable across the range	Balanced CNT–CB contribution; effective network
8% CNT/7% CB	~10^{-2}	Stable (frequency-independent)	CNT stabilizes the network; CB contribution is secondary
10% CNT/10% CB	~3×10^{-1}	Stable across the range	Well-formed conductive network; minimal frequency dependence
15% CNT/5% CB	~2	Stable (frequency-independent)	Very robust CNT-dominated network; highest conductivity
5% CNT/15% CB	~10^{-3}	Stable across the range	High CB but insufficient CNT; limited network efficiency

TABLE 6 | Comparison of electrical conductivity between SEBS and SEBS-MA composites across different CNT/CB loadings (corresponding to Figure 10).

Composite formulation	Conductivity (S/m)	Comparison (SEBS-MA vs. SEBS)	Interpretation
SEBS-MA/3% CNT/2% CB	Lower than SEBS/3% CNT/2% CB	SEBS-MA < SEBS	Maleic anhydride reduces conductivity at low loading
SEBS-MA/8% CNT/2% CB	$<10^{-2}$	SEBS-MA < SEBS ($>10^{-2}$)	SEBS shows higher network efficiency
SEBS-MA/10% CNT/5% CB	~1×10^{-1}	SEBS-MA < SEBS (~2×10^{-1})	CNT-rich SEBS is more conductive
SEBS-MA/15% CNT/5% CB	~1	SEBS-MA < SEBS (~2)	SEBS forms a more robust network at high loading

SEBS-MA composites show lower conductivity than elastomeric thermoplastic polymer (SEBS) composites, indicating that maleic anhydride modification does not improve the interaction between CNTs and the polymer matrix. Increasing CNT and CB concentrations, along with modifying elastomeric thermoplastic polymer (SEBS) to SEBS-MA, positively affects electrical conductivity, especially at higher frequencies. The balance between CNTs and CB can be optimized to achieve the desired conductivity and frequency response characteristics.

As the CNT content increases, the overall conductivity of the composites rises, and the frequency dependence decreases, indicating a shift toward a more stable, efficient conductive network dominated by CNTs. Conversely, higher CB content tends to lower the overall conductivity, reflecting less efficient network formation compared to CNTs. Increasing the proportion of CNTs significantly enhances overall conductivity and reduces frequency dependence, highlighting the role of CNTs in forming stable, efficient conductive networks within SEBS composites. The combination of CNTs and CB greatly influences the conductivity behavior of both SEBS and elastomeric thermoplastic polymer (SEBS) composites. Higher CNT content enhances conductivity and decreases frequency dependence, highlighting the importance of CNTs in establishing effective conductive networks. By adjusting the proportions of CNT and CB, the electrical properties of the composite can be tailored to specific requirements.

The electrical conductivity of filled SEBS and SEBS-MA composites follows the percolation scaling law for filler fractions above the critical threshold (ϕ_c). For CNT composites, loadings above approximately 3 wt% show a sharp increase in conductivity. SEBS/10 wt% CNT exhibits a stable plateau around 10^{-2} to 10^{-3} S·m^{-1}, while 16 wt% CNT reaches about 1 S·m^{-1}. For CB, the percolation threshold is much higher: composites with 10 wt% CB remain insulating, and only at 20 wt% does conductivity approach about 10^{-2} S·m^{-1}. These results confirm that the percolation threshold of CNT (> 3 wt%) is significantly lower than that of CB (> 12 wt%), highlighting the greater efficiency of CNT networks for electron transport. Figures 4–10 consistently support these threshold estimates.

Hybrid CNT/CB systems primarily function as CNT-controlled composites when the CNT content exceeds approximately 3 wt% of the total load. For instance, 7/3 and 8/2 wt% CNT/CB formulations already reach $\geq10^{-2}$ S·m^{-1} with only 8–10 wt% total filler. CB alone does not reduce the percolation threshold

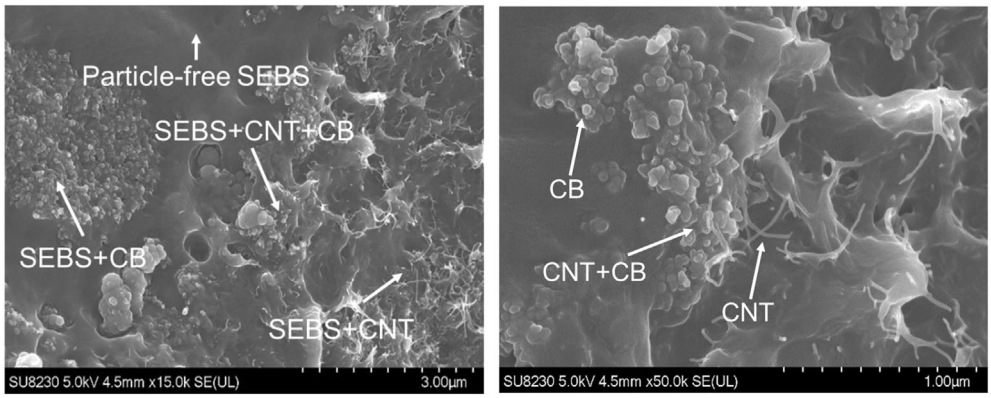

FIGURE 11 | Scanning electron micrograph of a multipin SEBS electrode reinforced with 10 wt% CNT and 5 wt% CB. Distinct regions are labeled: (i) particle-free SEBS matrix, (ii) CB + SEBS (agglomerated carbon black clusters), (iii) CNT + SEBS (fibrous nanotube networks), and (iv) CB + CNT + SEBS (mixed regions). The microstructure exhibits heterogeneous filler dispersion, with CNT networks forming conductive pathways and CB particles facilitating interfacial contacts, although some aggregation is observed.

independently. Matrix chemistry also affects conductivity. SEBS-MA consistently shows lower σ' than SEBS at the same loadings (e.g., 8/2, 10/5, and 15/5 wt% CNT/CB), implying either a slightly higher effective ϕ_c or lower network efficiency due to less favorable filler–matrix interactions. Therefore, maleic anhydride grafting does not positively shift the percolation threshold, though it may still enhance mechanical or interfacial properties. From a design standpoint, to achieve EEG-grade conductivity ($\sigma' \geq 10^{-2}\,S{\cdot}m^{-1}$ with minimal dispersion), CNT loadings should be kept at ≥ 7–8 wt%, with 2–3 wt% CB as a secondary filler. Formulations with high CB alone are not advised because their percolation threshold is well above 12 wt%, and conductivity gains are limited.

4.2 | Structural Properties

SEM was used to examine the morphology of the electrodes and the distribution of conductive fillers within the SEBS matrix. Figure 11 shows a micrograph of a multipin SEBS-based electrode reinforced with 10 wt% CNT and 5 wt% CB. Distinct regions are labeled to highlight filler dispersion: particle-free SEBS, CB + SEBS, CNT + SEBS, and CB + CNT + SEBS.

The particle-free SEBS areas represent the pure polymer matrix, characterized by smooth surfaces without filler inclusions. In contrast, the CB + SEBS regions display clusters of small, spherical, or irregularly shaped particles, indicating partial agglomeration of CB and suggesting limited uniformity in its dispersion. The CNT + SEBS regions show fibrous, entangled networks typical of CNTs, confirming the presence of extended conductive pathways that significantly contribute to percolation and charge transport. Finally, the CB + CNT + SEBS regions exhibit a combination of CB particles embedded within CNT entanglements, implying synergistic interactions where CB may bridge CNT bundles or improve filler–matrix interfacial contact. Overall, the micrograph shows a varied distribution of fillers within the SEBS matrix. While CB tends to form clusters, CNTs create interconnected fibrous networks, and their co-localization indicates some synergy between the two fillers. These structural observations directly relate to the electrical behavior discussed in Section 4.1, where CNT-dominated systems showed better conductivity and consistent performance across frequencies, while CB contributed less.

The SEM image in Figure 11 shows distinct phases within the SEBS/CB/CNT composite. CNTs appear as tangled, fibrous networks that create conductive pathways, which are vital for their electrical performance. In contrast, CB appears as clumped, spherical, or irregular particles, indicating limited dispersion within the matrix. While the CNT network supports efficient percolation, excessive entanglement can raise viscosity during processing. The hybrid CNT–CB regions suggest some synergistic interactions, where CB particles may enhance contact between CNT bundles. However, CB aggregation could reduce both electrical conductivity and mechanical strength. Overall, the SEM analysis shows an uneven distribution of fillers, with CNTs mainly contributing to conductivity and CB playing a smaller yet supportive role.

4.3 | Thermo-Mechanical Properties

TGA and DSC were performed to assess the thermal stability of SEBS and SEBS-MA composites reinforced with CNT and CB. The TGA verified the filler content and examined the decomposition behavior, while the DSC detected thermal transitions relevant to EEG operating conditions.

As shown in Figure 12 (TGA curves), all composites underwent a sharp weight loss starting around 350°C–400°C, which is typical of organic polymer degradation. After 400°C, the rate of mass loss increased sharply, indicating the beginning of the main decomposition phase of the polymer matrix. Both SEBS/16 wt% CNT and SEBS-MA/16 wt% CNT exhibited very similar degradation patterns, with weight loss starting within the same temperature range. After complete degradation, the remaining weights closely matched the expected CNT and CB loadings, confirming the proper addition of fillers.

Complementary DSC analyses (Figures 13 and 14) revealed a glass transition temperature (T_g) of approximately −60°C for both SEBS and SEBS-MA, indicating their elastomeric properties. No

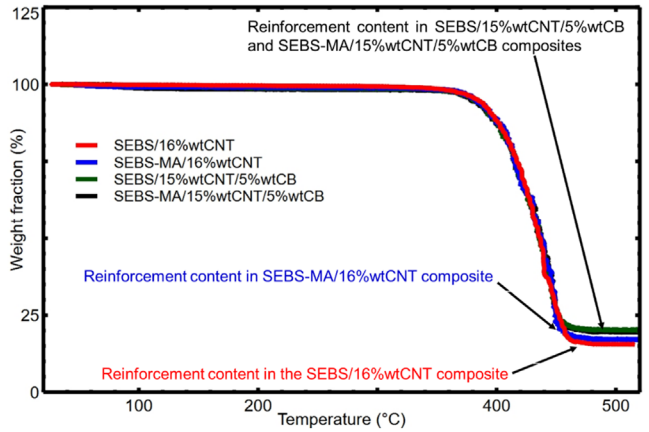

FIGURE 12 | Thermogravimetric analysis (TGA) curves of SEBS and SEBS-MA composites reinforced with CNT and CB. All samples exhibit a single significant decomposition step, starting around 350°C–400°C, which is typical of polymer matrix breakdown. The residual weights verify the intended CNT and CB loadings, with SEBS-MA/16 wt% CNT displaying a slightly higher residual percentage consistent with its reinforcement content. [Color figure can be viewed at wileyonlinelibrary.com]

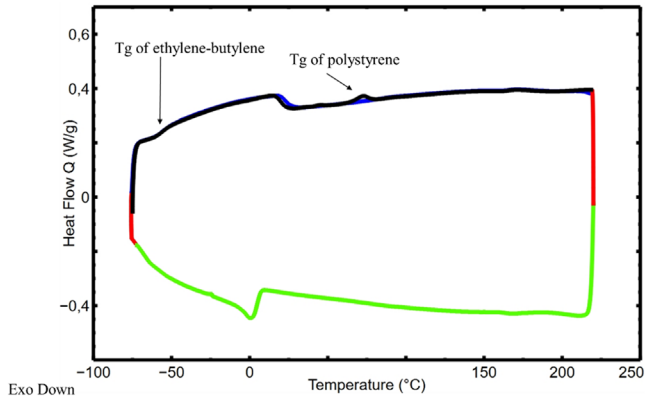

FIGURE 13 | The differential scanning calorimetry (DSC) curve of pure SEBS exhibits a glass transition temperature (T_g) of approximately −60°C, indicating its elastomeric properties. No melting or crystallization transitions occur within the physiological range of 24°C–36°C. [Color figure can be viewed at wileyonlinelibrary.com]

melting or crystallization transitions occur within the physiological temperature range (24°C–36°C). The PS phase exhibits a slightly higher transition range in SEBS (~90°C–100°C). The consistent T_g and degradation onset confirm that grafting maleic anhydride does not alter the core thermal behavior of the SEBS matrix.

Overall, the TGA and DSC results show that composites based on SEBS and SEBS-MA undergo a single main decomposition process, demonstrating high thermal stability with degradation starting only above 350°C. This temperature is well above the physiological range, ensuring that electrode performance remains unaffected during every day EEG use or extended skin contact. Importantly, confirming the filler content with TGA enhances the reliability of the electrical and mechanical properties reported in this study. While this work focused on

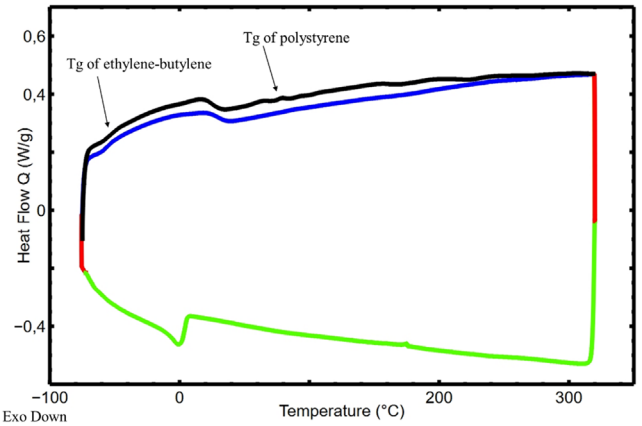

FIGURE 14 | Differential scanning calorimetry (DSC) curve of SEBS-MA. The glass transition temperature (T_g) occurs at about −60°C, the same as in neat SEBS, confirming that maleic anhydride grafting does not alter the primary thermal transition of the matrix. No melting or crystallization transitions are observed within the physiological temperature range (24°C–36°C). [Color figure can be viewed at wileyonlinelibrary.com]

the temperature range relevant to EEG, future studies could extend thermal analysis to assess behavior in other challenging environments. These results confirm that grafting does not alter the core elastomeric transition of the material; however, it can improve resistance at high temperatures while maintaining flexibility within the range relevant to EEG applications.

4.4 | DMTA

DMTA was conducted to assess the storage modulus (E') of SEBS and SEBS-MA composites within the physiological temperature range (24°C–36°C) at 1 Hz. This range was selected because the electrodes are designed for use at room and scalp temperatures. The storage modulus indicates the elastic response of the materials under dynamic loading, with higher values reflecting greater stiffness.

The results (Figure 15) show that neat SEBS has a higher storage modulus than SEBS-MA, confirming that grafting maleic anhydride improves the material's flexibility. Reinforcing with CNT and CB significantly increases the modulus in both matrices, and the storage modulus generally rises with more reinforcement content. Notably, all curves remain nearly flat across the tested range, indicating stable, solid-like behavior under EEG-relevant conditions. A detailed comparison of the relative storage modulus across formulations is summarized in Table 7.

Overall, maleic anhydride modification improves flexibility, while CNT and CB reinforcements increase stiffness. Among all formulations, SEBS-MA/8 wt% CNT/2 wt% CB emerges as the most promising for EEG electrodes, offering high conductivity combined with a low storage modulus similar to that of neat SEBS. This balance of softness and electrical performance is ideal for ensuring both comfort and reliable scalp contact during long-term EEG applications. Importantly, when considering the

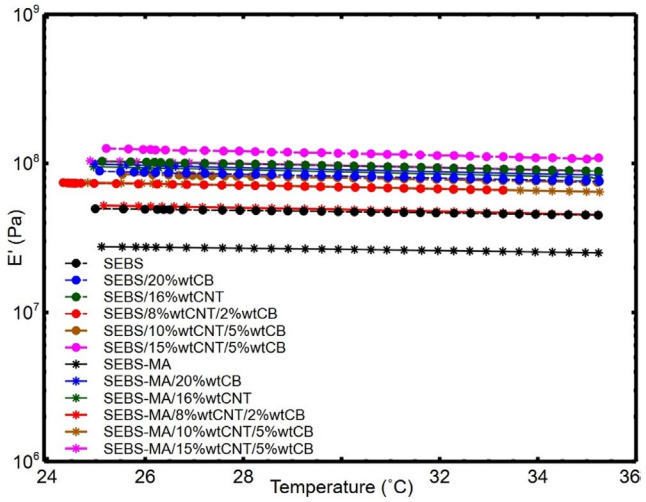

FIGURE 15 | Dynamic mechanical thermal analysis (DMTA) curves of SEBS and SEBS-MA composites (24°C–36°C, 1 Hz). The storage modulus (E') increases with CNT and CB reinforcement, while SEBS-MA-based composites show a lower modulus than SEBS, confirming increased flexibility. [Color figure can be viewed at wileyonlinelibrary.com]

TABLE 7 | Comparison of storage modulus (E') for SEBS and SEBS-MA composites (24°C–36°C, 1 Hz).

Material	Relative storage modulus (E')
SEBS	Higher than SEBS-MA; stiffer base polymer
SEBS-MA	Lower than SEBS; more flexible, softer base polymer
SEBS/20 wt% CB	Slightly lower than SEBS-MA/20 wt% CB; MA-modified version slightly stiffer
SEBS/16 wt% CNT	Slightly higher than SEBS-MA/16 wt% CNT
SEBS/8 wt% CNT/2 wt% CB	Higher than SEBS-MA/8 wt% CNT/2 wt% CB
SEBS-MA/8 wt% CNT/2 wt% CB	Similar to SEBS; most flexible conductive composite; optimal balance of properties
SEBS/10 wt% CNT/5 wt% CB	Higher than SEBS-MA/10 wt% CNT/5 wt% CB
SEBS-MA/10 wt% CNT/5 wt% CB	Similar to SEBS/8 wt% CNT/2 wt% CB
SEBS/15 wt% CNT/5 wt% CB	Higher than SEBS-MA/15 wt% CNT/5 wt% CB

DSC and TGA results, these findings confirm that the composites not only stay mechanically stable across the physiological range but also have excellent thermal stability well above typical operating conditions, reaffirming their suitability for safe and reliable EEG use.

4.5 | Preliminary In Vivo Validation

The contact impedance of the SEBS/8 wt% CNT/2 wt% CB electrode is 4.25 ± 0.5 kΩ, slightly lower than that of commercial flexible electrodes (4.75 ± 1.5 kΩ). The SEBS-MA/8 wt% CNT/2 wt% CB electrode shows a contact impedance of 4.5 ± 0.6 kΩ, placing it between the SEBS-based electrode and the commercial option. Based on these results, we can conclude that both SEBS-based electrodes are suitable for EEG applications, as they have contact impedance values comparable to those of commercial flexible electrodes (4.75 ± 1.5 kΩ), indicating their potential for similar electrical performance. The SEBS/8 wt% CNT/2 wt% CB electrode exhibits the lowest impedance (4.25 ± 0.5 kΩ), likely due to its higher electrical conductivity, which improves the electrode–skin interface and may reduce signal loss, thereby enhancing quality. The SEBS-MA/8 wt% CNT/2 wt% CB electrode has a slightly higher impedance (4.5 ± 0.6 kΩ), possibly because maleic anhydride modification affects composite dispersion or interfacial properties. Since EEG electrodes need low and stable contact impedance to prevent signal degradation, both SEBS-based electrodes show promise as alternatives to commercial flexible electrodes. Figure 16 displays EEG time-domain recordings of a commercial dry flexible electrode at position 2, compared to SEBS-MA/8 wt% CNT/2 wt% CB and SEBS/8 wt% CNT/2 wt% CB at positions 1 and 3, respectively, when the subject's eyes were open.

Figure 17 shows a typical EEG time-domain recording captured while the subject's eyes were open and blinking. The data highlight characteristic artifacts caused by eye blinks, which are essential to identify and manage during EEG data processing. The signal from the SEBS/8 wt% CNT/2 wt% CB electrode exhibits moderate amplitude fluctuations but remains relatively

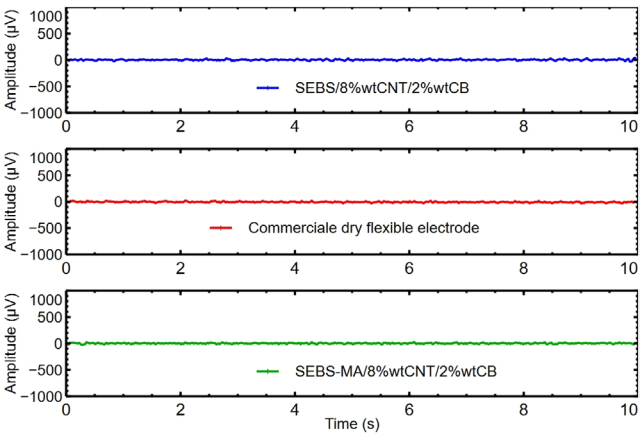

FIGURE 16 | Time-domain electroencephalography (EEG) recording during eyes-open condition. [Color figure can be viewed at wileyonlinelibrary.com]

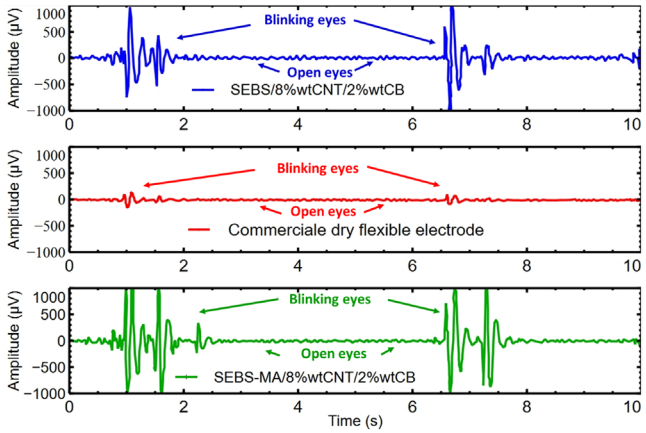

FIGURE 17 | Time-domain electroencephalography (EEG) recording during eyes-open with blinking. [Color figure can be viewed at wileyonlinelibrary.com]

stable, indicating that it records EEG data of acceptable quality. The signal from the commercial electrode is also stable, showing similar performance. Additionally, the signal from the SEBS-MA/8 wt% CNT/2 wt% CB electrode remains stable with minimal noise and fluctuations.

The transitions between different states (eyes-open and closed) are clearly visible, indicating the electrode's sensitivity to changes in mental state. The signal from the commercial electrode remains stable during these transitions, showing consistent performance. Meanwhile, the signal from the SEBS-MA/8 wt% CNT/2 wt% CB electrode is clear and effectively handles the transitions between open and closed states. This performance further confirms that SEBS-MA/8 wt% CNT/2 wt% CB is a promising choice for flexible, high-performance EEG electrodes, offering an ideal balance of conductivity and flexibility.

5 | Discussion

This study demonstrates that composites based on SEBS and SEBS-MA are promising options for flexible dry EEG electrodes, offering a new alternative to PDMS- and TPU-based matrices. SEBS and SEBS-MA maintain a favorable balance of conductivity, flexibility, and stability, illustrating the innovative application of these materials in EEG devices.

The role of CNTs in increasing conductivity was clearly observed. Their high aspect ratio enables the efficient formation of a percolated network, significantly reducing impedance once the percolation threshold is reached. However, adding more CNTs has disadvantages: excessive amounts can lead to agglomeration, poor dispersion, and higher processing viscosity, which can make the composite stiffer and decrease electrode comfort. Additionally, improvements in conductivity often plateau at higher CNT levels, indicating that network density, not just the amount of CNTs, is the critical factor. The addition of CB further boosts network connectivity by bridging gaps between nanotubes, creating a synergistic effect at optimal CNT/CB ratios. Recent literature has reported significant progress in conductive polymer composites, with a focus on multifunctional performance and interfacial optimization. For example, C. Liu et al. [52] and Y. Liu et al. [53] demonstrated self-healing CNT-based elastomers and PDMS-CNT composites with ultralow percolation thresholds, respectively. Gui et al. [54] and Lee et al. [55] reported hierarchical CNT/MXene and π-conjugated polymer/CNT systems with improved conductivity and EMI shielding. Likewise, Ye et al. [56] revealed how amorphous/crystalline heterophase structures enhance fatigue resistance. Together, these findings support the current results by demonstrating that continuous hybrid networks and optimized filler–matrix interactions are crucial for achieving simultaneous electrical conductivity, flexibility, and mechanical resilience. The hybrid SEBS-MA/CNT/CB composites in this study align with this design philosophy, demonstrating stable conductivity and flexibility suitable for wearable EEG applications.

SEBS-MA composites showed lower conductivity than their SEBS counterparts, likely due to changes in filler–matrix interactions caused by maleic anhydride grafting. However, the SEBS-MA/8 wt% CNT/2 wt% CB formulation exhibited stable conductivity and mechanical flexibility, as confirmed by DMTA results, which revealed a consistent storage modulus across the physiological temperature range. These properties are crucial for EEG electrodes that must remain flexible and reliable during long-term recordings. Notably, the transition temperatures found in this study closely match those reported in the literature for SEBS and SEBS-MA systems [57–59].

Additionally, the compression properties of SEBS-based composites have been thoroughly characterized in our previous work, providing complementary insights into their mechanical response under load. Cyclic compression tests conducted according to ASTM D575-91 on SEBS/20 wt% CB and EVA (ethylene-vinyl acetate)/20 wt% CB composites showed distinct behaviors: while EVA, a thermoplastic copolymer of ethylene and vinyl acetate, exhibited higher stiffness (elastic modulus ≈ 63.8 MPa; stress at 50% strain ≈ 16.2 MPa), the SEBS/20 wt% CB composite displayed lower stiffness (elastic modulus ≈ 47.2 MPa; stress ≈ 9.35 MPa) and greater deformability. These results confirm the inherent softness and elasticity of the SEBS matrix, key advantages for wearable and skin-contact sensors. Based on these findings and the DMTA results for pristine SEBS and SEBS-MA presented in Section 4.4, SEBS-MA is unlikely to differ substantially in compressive behavior from SEBS, as maleic anhydride grafting mainly improves polymer–filler interfacial adhesion and slightly enhances flexibility without significantly altering the bulk modulus. Consequently, the compressive mechanical performance of SEBS-MA composites can be reliably inferred from the SEBS data obtained in our previous study.

Regarding storage modulus, most past studies have analyzed these materials at temperatures well above those relevant to EEG operation. In contrast, this study specifically examined the physiological range (24°C–36°C), the same range used in many other studies [60–62], providing more realistic insights into electrode behavior under actual use conditions.

Together, the DSC and TGA results confirm that SEBS and SEBS-MA composites stay thermally stable under EEG-relevant conditions (room and scalp temperatures). The degradation begins at around 400°C, providing a large safety margin, which ensures that electrode performance is not affected by physiological

heating or prolonged skin contact. The TGA profiles also confirmed filler incorporation and showed consistent thermal stability across all formulations. The minor differences in storage modulus between SEBS and SEBS-MA suggest that maleic anhydride functionalization may slightly improve flexibility without sacrificing thermal stability. Although this study focused on the physiological temperature range relevant to EEG, additional thermal analyses could further clarify how the materials behave during sterilization, storage, and processing, which will be explored in future work.

Preliminary in vivo EEG validation showed that SEBS/8 wt% CNT/2 wt% CB and SEBS-MA/8 wt% CNT/2 wt% CB electrodes provided clearer transitions and more stable signals compared to a commercial dry electrode, with the latter demonstrating the most consistent performance. Although promising, these results should be regarded as initial, given the small number of participants, and further validation with larger groups is necessary before making broader claims.

The contact impedance achieved in this study is significantly lower than that of most PDMS- and TPU-based dry electrodes reported in the literature. Commercial and experimental electrodes using these soft matrices typically show impedance values between 10 kΩ and 600 kΩ, depending on fabrication and testing conditions [20, 27, 44, 63, 64]. In contrast, the SEBS/CNT/CB and SEBS-MA/CNT/CB hybrid electrodes developed here achieved impedance values below 5 kΩ, demonstrating a significant improvement in electrical performance. This result highlights the efficiency of the hybrid conductive network and the SEBS-based matrix in ensuring intimate skin contact, effective charge transfer, and stable EEG signal acquisition while preserving flexibility and comfort.

Despite promising results, this study has some limitations. The in vivo validation was preliminary, involving a small sample size of participants and only time-domain analysis. Future research should include larger groups, frequency-domain assessments, and long-term testing for comfort, durability, and electrode–skin interactions. Additionally, improving CNT dispersion methods could reduce agglomeration at higher loadings, enabling better conductivity without sacrificing flexibility. Addressing these issues will be crucial for establishing SEBS- and SEBS-MA-based composites as reliable next-generation materials for dry EEG electrodes.

6 | Conclusion

This study shows that composites based on SEBS and SEBS-MA, reinforced with CNT and CB, are promising options for flexible dry EEG electrodes. Notably, SEBS-MA/8 wt% CNT/2 wt% CB achieved a low contact impedance of 4.5 ± 0.6 kΩ, similar to commercial flexible electrodes and close to SEBS/8 wt% CNT/2 wt% CB, which measured 4.25 ± 0.5 kΩ. The composite maintained a storage modulus comparable to that of pure SEBS, confirming high flexibility while providing enough stiffness for stable scalp contact. Initial in vivo EEG tests further demonstrated that both SEBS and SEBS-MA composites generated stable signals with accurate detection of brain state changes, outperforming EVA/CB electrodes in terms of noise reduction and stability.

Although these results are encouraging, some limitations need to be acknowledged. The in vivo validation was preliminary, involving a small sample size and limited to time-domain analysis. Larger studies and frequency-domain assessments are necessary to establish broader clinical relevance. SEBS-MA composites also showed a slight decrease in conductivity compared to SEBS, indicating a compromise between electrical performance and increased stiffness. Furthermore, large-scale reproducibility might be influenced by the dispersion and agglomeration of CNTs, which require careful optimization of processing conditions.

In summary, SEBS- and SEBS-MA-based nanocomposites demonstrate strong potential as next-generation EEG electrodes, offering a better balance of conductivity, flexibility, and stability compared to PDMS- or TPU-based options. However, further validation and process improvements are necessary to turn these materials into reliable, scalable devices for practical EEG applications.

A comprehensive quantitative percolation modeling study will be conducted in future research for each hybrid system to quantify the percolation thresholds better and understand the relationship between filler content, network formation, and electrical conductivity.

Author Contributions

George Gnonhoue: conceptualization (lead), formal analysis (lead), investigation (lead), methodology (lead), project administration (lead), validation (lead), writing – original draft (lead), writing – review and editing (lead). **Éric David:** conceptualization (lead), funding acquisition (lead), project administration (lead), validation (lead), writing – review and editing (lead). **Jérémie Voix:** conceptualization (lead), funding acquisition (lead), supervision (lead), validation (lead), writing – review and editing (lead). **Ilyass Tabiai:** conceptualization (lead), funding acquisition (lead), project administration (lead), supervision (lead).

Acknowledgments

The authors acknowledge the financial support from the Natural Sciences and Engineering Research Council (NSERC) Alliance (ALLRP 566678-2021), Mitacs IT26677 (SUBV-2021-168), and PROMPT (#164_Voix-EERS 2021.06) for the École de Technologie Supérieure—Ear and Auditory Research Group (ÉTS-EERS) Industrial Research Chair in Ear Technologies, sponsored by Ear and Auditory Research Group (EERS) Global Technologies Inc.

Funding

This work was supported by Natural Sciences and Engineering Research Council of Canada (Grant No. ALLRP 566678-2021), Mitacs (Grant No. MITACS IT26677 (SUBV-2021-168)), and PROMPT (Grant No. #164_Voix-EERS 2021.06).

Conflicts of Interest

The authors declare no conflicts of interest.

Data Availability Statement

The data that support the findings of this study are available on request from the corresponding author. The data are not publicly available due to privacy or ethical restrictions.

References

1. M. Arai, Y. Nishinaka, and N. Miki, "Electroencephalogram Measurement Using Polymer-Based Dry Microneedle Electrode," *Japanese Journal of Applied Physics* 54, no. 6S1 (2015): 06FP14, https://doi.org/10.7567/JJAP.54.06FP14.

2. L. T. Cunha, P. Pedrosa, C. J. Tavares, E. Alves, F. Vaz, and C. Fonseca, "The Role of Composition, Morphology and Crystalline Structure in the Electrochemical Behaviour of TiN_x Thin Films for Dry Electrode Sensor Materials," *Electrochimica Acta* 55, no. 1 (2009): 59–67, https://doi.org/10.1016/j.electacta.2009.08.004.

3. Y. Fu, J. Zhao, Y. Dong, and X. Wang, "Dry Electrodes for Human Bioelectrical Signal Monitoring," *Sensors* 20, no. 13 (2020): 3651, https://doi.org/10.3390/s20133651.

4. S. Krachunov and A. Casson, "3D Printed Dry EEG Electrodes," *Sensors* 16, no. 10 (2016): 1635, https://doi.org/10.3390/s16101635.

5. H. Hinrichs, M. Scholz, A. K. Baum, J. W. Y. Kam, R. T. Knight, and H.-J. Heinze, "Comparison Between a Wireless Dry Electrode EEG System With a Conventional Wired Wet Electrode EEG System for Clinical Applications," *Scientific Reports* 10, no. 1 (2020): 5218, https://doi.org/10.1038/s41598-020-62154-0.

6. G. Li, S. Wang, and Y. Y. Duan, "Towards Conductive-Gel-Free Electrodes: Understanding the Wet Electrode, Semi-Dry Electrode and Dry Electrode-Skin Interface Impedance Using Electrochemical Impedance Spectroscopy Fitting," *Sensors and Actuators B: Chemical* 277 (2018): 250–260, https://doi.org/10.1016/j.snb.2018.08.155.

7. G. Petrossian, P. Kateb, F. Miquet-Westphal, and F. Cicoira, "Advances in Electrode Materials for Scalp, Forehead, and Ear EEG: A Mini-Review," *ACS Applied Bio Materials* 6, no. 8 (2023): 3019–3032, https://doi.org/10.1021/acsabm.3c00322.

8. R. Wang, X. Jiang, W. Wang, and Z. Li, "A Microneedle Electrode Array on Flexible Substrate for Long-Term EEG Monitoring," *Sensors and Actuators B: Chemical* 244 (2017): 750–758, https://doi.org/10.1016/j.snb.2017.01.052.

9. J. Li, Y. Ma, D. Huang, et al., "High-Performance Flexible Microneedle Array as a Low-Impedance Surface Biopotential Dry Electrode for Wearable Electrophysiological Recording and Polysomnography," *Nano-Micro Letters* 14, no. 1 (2022): 132, https://doi.org/10.1007/s40820-022-00870-0.

10. B. Babusiak, S. Borik, and L. Balogova, "Textile Electrodes in Capacitive Signal Sensing Applications," *Measurement* 114 (2018): 69–77, https://doi.org/10.1016/j.measurement.2017.09.024.

11. H. J. Baek, H. J. Lee, Y. G. Lim, and K. S. Park, "Conductive Polymer Foam Surface Improves the Performance of a Capacitive EEG Electrode," *IEEE Transactions on Biomedical Engineering* 59, no. 12 (2012): 3422–3431, https://doi.org/10.1109/TBME.2012.2215032.

12. Y. Gao, V. V. Soman, J. P. Lombardi, et al., "Heart Monitor Using Flexible Capacitive ECG Electrodes," *IEEE Transactions on Instrumentation and Measurement* 69, no. 7 (2020): 4314–4323, https://doi.org/10.1109/TIM.2019.2949320.

13. S. M. Lee, J. H. Kim, H. J. Byeon, Y. Y. Choi, K. S. Park, and S.-H. Lee, "A Capacitive, Biocompatible and Adhesive Electrode for Long-Term and Cap-Free Monitoring of EEG Signals," *Journal of Neural Engineering* 10, no. 3 (2013): 036006, https://doi.org/10.1088/1741-2560/10/3/036006.

14. S. M. Lee, J. H. Kim, C. Park, et al., "Self-Adhesive and Capacitive Carbon Nanotube-Based Electrode to Record Electroencephalograph Signals From the Hairy Scalp," *IEEE Transactions on Biomedical Engineering* 63, no. 1 (2016): 138–147, https://doi.org/10.1109/TBME.2015.2478406.

15. X. Cheng, C. Bao, X. Wang, F. Zhang, and W. Dong, "Soft Surface Electrode Based on PDMS-CB Conductive Polymer for Electrocardiogram Recordings," *Applied Physics A* 125, no. 12 (2019): 876, https://doi.org/10.1007/s00339-019-3124-5.

16. L. Yang, L. Gan, Z. Zhang, et al., "Insight Into the Contact Impedance Between the Electrode and the Skin Surface for Electrophysical Recordings," *ACS Omega* 7, no. 16 (2022): 13906–13912, https://doi.org/10.1021/acsomega.2c00282.

17. A. Asayesh, I. F. Warsito, J. Haueisen, P. Fiedler, and S. Vanhatalo, "Neonatal Electroencephalogram Recording With a Dry Electrode Cap: A Feasibility Study," *Sensors* 25, no. 3 (2025): 966, https://doi.org/10.3390/s25030966.

18. P. Fiedler, U. Graichen, E. Zimmer, and J. Haueisen, "Simultaneous Dry and Gel-Based High-Density Electroencephalography Recordings," *Sensors* 23, no. 24 (2023): 9745, https://doi.org/10.3390/s23249745.

19. P. Fiedler, R. Muhle, S. Griebel, et al., "Contact Pressure and Flexibility of Multipin Dry EEG Electrodes," *IEEE Transactions on Neural Systems and Rehabilitation Engineering* 26, no. 4 (2018): 750–757, https://doi.org/10.1109/TNSRE.2018.2811752.

20. P. Fiedler, P. Pedrosa, S. Griebel, et al., "Novel Multipin Electrode Cap System for Dry Electroencephalography," *Brain Topography* 28, no. 5 (2015): 647–656, https://doi.org/10.1007/s10548-015-0435-5.

21. P. Fiedler, P. Pedrosa, S. Griebel, et al., "Novel Flexible Dry PU/TiN-Multipin Electrodes: First Application in EEG Measurements," *Annual International Conference of the IEEE Engineering in Medicine and Biology Society* 2011 (2011): 55–58, https://doi.org/10.1109/IEMBS.2011.6089895.

22. P. Fiedler, D. Strohmeier, A. Hunold, et al., "Modular Multipin Electrodes for Comfortable Dry EEG," in *2016 38th Annual International Conference of the IEEE Engineering in Medicine and Biology Society (EMBC)* (2016), 5705–5708.

23. I. F. Warsito, M. Komosar, M. A. Bernhard, P. Fiedler, and J. Haueisen, "Flower Electrodes for Comfortable Dry Electroencephalography," *Scientific Reports* 13, no. 1 (2023): 16589, https://doi.org/10.1038/s41598-023-42732-8.

24. J. Hoon Lee, S. Min Lee, H. Jin Byeon, J. Sook Hong, K. Suk Park, and S.-H. Lee, "CNT/PDMS-Based Canal-Typed Ear Electrodes for Inconspicuous EEG Recording," *Journal of Neural Engineering* 11, no. 4 (2014): 046014, https://doi.org/10.1088/1741-2560/11/4/046014.

25. J. S. Heo, M. F. Hossain, and I. Kim, "Challenges in Design and Fabrication of Flexible/Stretchable Carbon- and Textile-Based Wearable Sensors for Health Monitoring: A Critical Review," *Sensors* 20, no. 14 (2020): 3927, https://doi.org/10.3390/s20143927.

26. Y. Wang, X. Wang, L. Sandsjö, X. Liu, and L. Guo, "Deploying Partially Cross-Linked Elastomers to Optimize Adhesion for Long-Term Surface Electromyography Electrodes," *Advanced Materials Interfaces* 12 (2025): 2400757, https://doi.org/10.1002/admi.202400757.

27. J. Oh, K.-W. Nam, W.-J. Kim, B.-H. Kang, and S.-H. Park, "Flexible Dry Electrode Based on a Wrinkled Surface That Uses Carbon Nanotube/Polymer Composites for Recording Electroencephalograms," *Materials* 17, no. 3 (2024): 668, https://doi.org/10.3390/ma17030668.

28. K. Alavi, S. Tarashi, H. Nazockdast, and M. Rafizadeh, "Microstructure Development and Mechanical Performance of MWCNTs/GNPs Filled SEBS With Different Block Content," *Polymer Composites* 44, no. 11 (2023): 8125–8140, https://doi.org/10.1002/pc.27693.

29. V. Aravinth, V. Navaneethakrishnan, S. Vishvanathperumal, and G. Gurumoorthi, "Effect of Modified Nanographene Oxide (mGO)/Carbon Nanotubes (CNTs) Hybrid Filler on the Cure, Mechanical and Swelling Properties of Silicone Rubber Composites," *Journal of Inorganic and Organometallic Polymers and Materials* 34, no. 1 (2024): 282–301, https://doi.org/10.1007/s10904-023-02818-2.

30. Y. Cai, D. Chen, L. Cheng, et al., "Preparation and Sensing Properties of Multiscale Conductive Filler Hybrid CNTs@Ag-MXene-TPU/TPU Double-Layer Strain Sensing Materials," *Composites Part A: Applied Science and Manufacturing* 186 (2024): 108430, https://doi.org/10.1016/j.compositesa.2024.108430.

31. W. He, J. Ma, L. Kang, L. Wang, and M. Zhu, "Highly Sensitive and Stretchable CB/GNPs-TPU Strain Sensor With Porous Microstructure for Multifunctional Strain Sensing," *Materials Today Communications* 41 (2024): 110800, https://doi.org/10.1016/j.mtcomm.2024.110800.

32. J.-W. Li, H.-F. Chen, Y.-Z. Liu, J.-H. Wang, M.-C. Lu, and C.-W. Chiu, "Photocurable 3D-Printed AgNPs/Graphene/Polymer Nanocomposites With High Flexibility and Stretchability for ECG and EMG Smart Clothing," *Chemical Engineering Journal* 484 (2024): 149452, https://doi.org/10.1016/j.cej.2024.149452.

33. Y. Yao, H. Dai, M. Ji, et al., "Flexible Strain Sensor Based on AgNWs/MXene/SEBS With High Sensitivity and Wide Strain Range," *Electronic Materials Letters* 20, no. 6 (2024): 684–693, https://doi.org/10.1007/s13391-024-00514-y.

34. V. Kumar, A. Manikkavel, M. A. Yewale, M. N. Alam, and S.-S. Park, "Lightweight, Compressible, Stretchable, Ultra-Soft, and Mechanically Stable Composites for Piezo-Electric Energy Generators and Strain Sensing," *Materials Research Bulletin* 179 (2024): 112962, https://doi.org/10.1016/j.materresbull.2024.112962.

35. S. Lv, Z. Cao, Z. Ying, et al., "Flexible, Stretchable, Wearable Electronic Skins Based on Aligned Carbon Nanotube Fiber Arrays for Motion Detection and Human–Machine Interaction," *Sensors and Actuators A: Physical* 362 (2023): 114634, https://doi.org/10.1016/j.sna.2023.114634.

36. R. Mahato, S. Masiul Islam, and S. Singh, "Flexible Piezo-Resistive Strain Sensors Based on Silver Nanowires and Graphene Nanoplatelets Reinforced Polydimethylsiloxane for Human Motion Detection," *Materials Today Communications* 40 (2024): 110056, https://doi.org/10.1016/j.mtcomm.2024.110056.

37. S. J. Paul, S. Srivastava, J. S. Tawale, and B. K. Gupta, "Three-Dimensional CNT-rGO/PDMS Porous Scaffold Derived Supercompressible Lightweight Body-Mounted Piezoresistive Force Sensor for Human Motion Monitoring," *Colloids and Surfaces A: Physicochemical and Engineering Aspects* 675 (2023): 131993, https://doi.org/10.1016/j.colsurfa.2023.131993.

38. R. Promsung, A. Georgopoulou, Y. Nakaramontri, E. Kalkornsurapranee, and F. Clemens, "Piezoresistive Properties for Soft Structures Using Hybrid CCB/CNT-Based Natural Rubber Latex Composites," *Applied Materials Today* 39 (2024): 102302, https://doi.org/10.1016/j.apmt.2024.102302.

39. S. Shajari, S. Ramakrishnan, K. Karan, L. J. Sudak, and U. Sundararaj, "Ultrasensitive Wearable Sensor With Novel Hybrid Structures of Silver Nanowires and Carbon Nanotubes in Fluoroelastomer: Multi-Directional Sensing for Human Health Monitoring and Stretchable Electronics," *Applied Materials Today* 26 (2022): 101295, https://doi.org/10.1016/j.apmt.2021.101295.

40. J. Wang, S. Li, L. Yang, et al., "Graphene-Based Hybrid Fillers for Rubber Composites," *Molecules* 29, no. 5 (2024): 1009, https://doi.org/10.3390/molecules29051009.

41. S. Xu, X. Li, G. Sui, R. Du, Q. Zhang, and Q. Fu, "Plasma Modification of PU Foam for Piezoresistive Sensor With High Sensitivity, Mechanical Properties and Long-Term Stability," *Chemical Engineering Journal* 381 (2020): 122666, https://doi.org/10.1016/j.cej.2019.122666.

42. L.-F. Wang, J.-Q. Liu, B. Yang, and C.-S. Yang, "PDMS-Based Low Cost Flexible Dry Electrode for Long-Term EEG Measurement," *IEEE Sensors Journal* 12, no. 9 (2012): 2898–2904, https://doi.org/10.1109/JSEN.2012.2204339.

43. Z. Wang, C. Chen, W. Li, et al., "A Multichannel EEG Acquisition System With Novel Ag NWs/PDMS Flexible Dry Electrodes," *Annual International Conference of the IEEE Engineering in Medicine and Biology Society* 2018 (2018): 1299–1302, https://doi.org/10.1109/EMBC.2018.8512563.

44. J. J. A. Heijs, R. J. Havelaar, P. Fiedler, R. J. A. Van Wezel, and T. Heida, "Validation of Soft Multipin Dry EEG Electrodes," *Sensors* 21, no. 20 (2021): 6827, https://doi.org/10.3390/s21206827.

45. B. Vasconcelos, P. Fiedler, R. Machts, J. Haueisen, and C. Fonseca, "The Arch Electrode: A Novel Dry Electrode Concept for Improved Wearing Comfort," *Frontiers in Neuroscience* 15 (2021): 748100, https://doi.org/10.3389/fnins.2021.748100.

46. T. Chen, G. Wu, M. Panahi-Sarmad, et al., "A Novel Flexible Piezoresistive Sensor Using Superelastic Fabric Coated With Highly Durable SEBS/TPU/CB/CNF Nanocomposite for Detection of Human Motions," *Composites Science and Technology* 227 (2022): 109563, https://doi.org/10.1016/j.compscitech.2022.109563.

47. M. Liu, Y. Sheng, C. Huang, et al., "Highly Stretchable and Sensitive SBS/gr/CNTs Fibers With Hierarchical Structure for Strain Sensors," *Composites Part A: Applied Science and Manufacturing* 164 (2023): 107296, https://doi.org/10.1016/j.compositesa.2022.107296.

48. B. Zhou, Z. Liu, C. Li, et al., "Fabrication of Ultrasensitive and Flexible Strain Sensor Based on Multi-Wall Carbon Nanotubes Coated Electrospun Styrene-Ethylene-Butylene-Styrene Block Copolymer Fibrous Tubes," *European Polymer Journal* 178 (2022): 111501, https://doi.org/10.1016/j.eurpolymj.2022.111501.

49. E. Alikhani and M. Mohammadi, "EVA and SEBS-MA Copolymers Incorporated Silicone Rubber/SEBS Blends: Improvement of Mechanical and Thermal Properties," *Scientific Reports* 13, no. 1 (2023): 22596, https://doi.org/10.1038/s41598-023-49796-6.

50. R. M. Grigorescu, F. Ciuprina, P. Ghioca, et al., "Mechanical and Dielectric Properties of SEBS Modified by Graphite Inclusion and Composite Interface," *Journal of Physics and Chemistry of Solids* 89 (2016): 97–106, https://doi.org/10.1016/j.jpcs.2015.10.008.

51. S. R. Sinha, L. Sullivan, D. Sabau, et al., "American Clinical Neurophysiology Society Guideline 1: Minimum Technical Requirements for Performing Clinical Electroencephalography," *Journal of Clinical Neurophysiology* 33, no. 4 (2016): 303–307, https://doi.org/10.1097/WNP.0000000000000308.

52. C. Liu, Y. Cai, T. Liang, T. Zang, G. Fei, and H. Xia, "Additive Manufacturing Flexible, Conductive and Self-Healing Polydimethylsiloxane Carbon Nanotubes Composites for Electromagnetic Interference Shielding and Microwave Absorption," *Chemical Engineering Journal* 520 (2025): 165717, https://doi.org/10.1016/j.cej.2025.165717.

53. Y. Liu, X. Wu, H. Zhang, et al., "Self-Healing Poly(Siloxane-Urethane) Carbon Nanotube Composites With Multi-Band Repairing Capability and Efficient Recovery Have Significant Photothermal Response," *Colloid and Polymer Science* 303, no. 8 (2025): 1681–1693, https://doi.org/10.1007/s00396-025-05450-3.

54. H. Gui, X. Zhao, S. Zuo, et al., "Carbonized Syndiotactic Polystyrene/Carbon Nanotube/MXene Hybrid Aerogels With Egg-Box Structure: A Platform for Electromagnetic Interference Shielding and Solar Thermal Energy Management," *ACS Applied Materials & Interfaces* 15, no. 33 (2023): 39740–39751, https://doi.org/10.1021/acsami.3c08176.

55. Y.-H. Lee, C.-L. Wu, C.-W. Lai, and J.-X. Huang, "Thin, Lightweight, and Highly Efficient Electromagnetic Interference Shielding Nanocomposites Composed of a π-Conjugated Block Copolymer Nanowire/Multiwalled Carbon Nanotube Bicontinuous Interpenetrating Network," *ACS Omega* 10, no. 14 (2025): 14296–14305, https://doi.org/10.1021/acsomega.5c00452.

56. Z. Ye, T. Fang, C. Cong, et al., "Strong and Fatigue-Resistant Carbon Nanotube Composites Enabled by Amorphous/Crystalline Heterophase Shell," *ACS Nano* 18, no. 36 (2024): 24984–24996, https://doi.org/10.1021/acsnano.4c05966.

57. T. Aouissi, A. Hellati, A. Zerriouh, et al., "Compatibilization of Immiscible PLA/LDPE Blends Using SEBS-g-MAH: A Multiscale Approach Combining Experimental and Computational Studies," *Macromolecular Chemistry and Physics* 226, no. 18 (2025): e00137, https://doi.org/10.1002/macp.202500137.

58. N. G. Davidyants, I. Y. Gorbunova, S. V. Polunin, T. P. Kravchenko, and A. V. Khoroshilov, "Effect of SEBS-g-MA on Recycled PS/HDPE

Blend Miscibility," *Colloid and Polymer Science* 303, no. 6 (2025): 1139–1154, https://doi.org/10.1007/s00396-025-05407-6.

59. X. Li, Z. Wang, T. Liu, G. Li, Y. Wei, and X. Wang, "Mechanical and Electrical Properties of PP Composite Modified by SEBS Used for High Voltage Cable," *Engineering Fracture Mechanics* 315 (2025): 110807, https://doi.org/10.1016/j.engfracmech.2025.110807.

60. H. Honda and K. Nishiyama, "Anti-Shivering Drug Influences the Characteristics of Electroencephalographic Shivering Noise During Targeted Temperature Management: A Case Report," *Cureus* 17, no. 5 (2025): e84509, https://doi.org/10.7759/cureus.84509.

61. H. Wang, R. Yan, H. Lin, et al., "Improving Thermal Comfort and Cognitive Ability of Manual Workers by Cooling Garment of Different Temperatures Based on EEG Analysis," *Energy and Buildings* 331 (2025): 115371, https://doi.org/10.1016/j.enbuild.2025.115371.

62. Z. Wang, H. Yi, and Z. Li, "Body Temperature-Triggered Phase Change Dry Electrode for Long-Term Comfort Electroencephalography Monitoring," *National Science Open* 4, no. 2 (2025): 20240025, https://doi.org/10.1360/nso/20240025.

63. Z. Wang, Y. Ding, W. Yuan, H. Chen, W. Chen, and C. Chen, "Active Claw-Shaped Dry Electrodes for EEG Measurement in Hair Areas," *Bioengineering* 11, no. 3 (2024): 276, https://doi.org/10.3390/bioengineering11030276.

64. L. Xing and A. J. Casson, "3D-Printed, Directly Conductive and Flexible Electrodes for Personalized Electroencephalography," *Sensors and Actuators A: Physical* 349 (2023): 114062, https://doi.org/10.1016/j.sna.2022.114062.